Spectral Theory of Non-Markovian Dissipative Phase Transitions

Baptiste Debecker, John Martin, François Damanet[1]

[1] *Institut de Physique Nucléaire, Atomique et de Spectroscopie, CESAM, University of Liège, B-4000 Liège, Belgium*

(Dated: July 3, 2023)

To date, dissipative phase transitions (DPTs) have mostly been studied for quantum systems coupled to idealized Markovian (memoryless) environments, where the closing of the Liouvillian gap constitutes a hallmark. Here, we extend the spectral theory of DPTs to arbitrary non-Markovian systems and present a general and systematic method to extract their signatures, which is fundamental for the understanding of realistic materials and experiments such as in the solid-state, cold atoms, cavity or circuit QED. We first illustrate our theory to show how memory effects can be used as a resource to control phase boundaries in a model exhibiting a first-order DPT, and then demonstrate the power of the method by capturing all features of a challenging second-order DPT in a two-mode Dicke model for which previous attempts had fail up to now.

Introduction. Finding new ways to control phase transitions in quantum systems to access different properties is at the forefront of research for developing new materials and technologies. In this context, driven-dissipative mechanisms obtained via the coupling of systems to engineered environments and fields offer opportunities to generate matter phases otherwise inaccessible [1–3].

However, so far, dissipative phase transitions (DPTs) have mostly been studied for systems coupled to memoryless reservoirs [4–6]. Yet, most realistic systems are coupled to reservoirs with a spectral structure [7], giving the latter a memory of past system-bath exchanges, which considerably complicates their dynamics. Such non-Markovian effects are crucial to be understood, not least because they can be used as a resource to generate useful phenomena, such as non-Markovian-assisted steady state entanglement [8], quantum transport [9], spin squeezing [10], chaotic behaviors [11] or new dynamical phases [12]. Moreover, from a computational perspective, it is sometimes desirable to derive reduced descriptions of a large Markovian open quantum system in order to deal with a smaller Hilbert space, which usually implies dealing with non-Markovian effects [13, 14].

Here, we extend the spectral theory of DPTs to arbitrary non-Markovian systems and present a general method to characterize their signatures, opening possibilities for exploring DPTs in a wider range of systems. Our approach is based on the Hierarchical Equations of Motion (HEOM) [15–20], a numerical method for non-Markovian dynamics extensively used in quantum physics and chemistry, from which one can define a generalization of the Liouvillian usually associated with the Lindblad master equation for Markovian systems whose spectral properties are connected to DPTs. Indeed, one of the necessary conditions for DPTs is the closing of the Liouvillian gap [4]. To the best of our knowledge, we are the first to show that HEOM can be used to define a similar quantity for non-Markovian systems and derive a spectral theory of non-Markovian DPTs.

Non-Markovian effects in DPTs have been studied via other techniques, such as Green functions to study the impact of the environment spectral density on the critical exponent [21, 22], Lindblad master equations with time-dependent rates to characterize the dynamics of a probe coupled to a non-Markovian environment [23], or time-evolving matrix product operators (TEMPO) to localize DPT in the spin-boson model [24]. However, such studies are sparse and mostly focused on the paradigmatic spin-boson model [25–27]. As our approach is the natural extension of the powerful spectral theory machinery widely used for Markovian systems, it provides an ideal framework to complement previous studies and explore non-Markovian effects in new regimes and systems relevant for real materials and experiments.

Below, we first present the central element of this work: the generalization of the Liouvillian for non-Markovian systems. We then derive its properties and their connections with DPTs and symmetries. As a first example, we study a generalized Lipkin-Meshkov-Glick model [28] and show that deviations from a Markovian reservoir lead to a shift of the phase transition boundary. Finally, we show our framework can capture all the features of a DPT in a challenging two-mode Dicke model [14] for which all previous non-Markovian descriptions had fail so far.

Theoretical framework. We consider an arbitrary quantum system S linearly coupled to a bosonic environment E of harmonic oscillators at zero temperature, keeping in mind that the theory below is easily generalizable to multiple bosonic or fermionic baths at finite temperatures. The total Hamiltonian reads (we set $\hbar = 1$)

$$H = H_S + \underbrace{\sum_k \omega_k a_k^\dagger a_k}_{\equiv\, H_E} + \underbrace{\sum_k (g_k a_k L_k^\dagger + g_k^* a_k^\dagger L_k)}_{\equiv\, H_{\rm int}}, \quad (1)$$

where H_S is the system Hamiltonian, H_E is the environment Hamiltonian with a_k ($a_k^\dagger$) the annihilation (creation) operator for the k-th mode of frequency ω_k, and $H_{\rm int}$ is the interaction Hamiltonian with L_k being arbitrary system operators and g_k being the system-bath coupling strengths. The effect of the environment

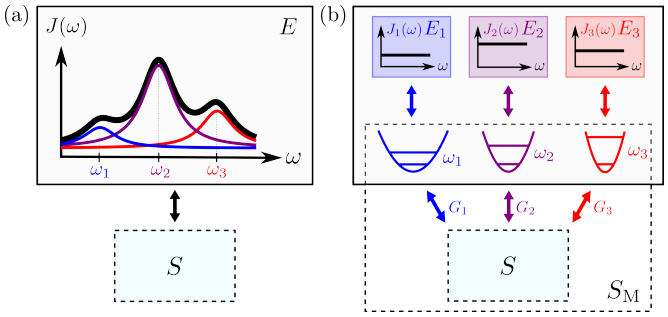

FIG. 1. (a): General sketch of a system S interacting with a structured environment E characterized by a specified spectral density $J(\omega)$ which can be decomposed into three Lorentzians, as if the system was coupled to three pseudo-modes coupled to their own unstructured bath (b). If one enlarges the system S by including the pseudo-modes (system S_M in the dashed black box), the dynamics can be treated by a standard Lindblad description.

on the system is encoded in the spectral density (SD) $J(\omega) = \pi \sum_k |g_k|^2 \delta(\omega - \omega_k)$ or equivalently in the bath correlation function (CF) $\alpha(\tau) = \sum_k |g_k|^2 e^{-i\omega_k \tau}$ which are related to each other in the continuum limit via the relation $\alpha(\tau) = (1/\pi)\int_0^\infty J(\omega) e^{i\omega\tau} \mathrm{d}\omega$. The SD is a positive function whose specific structure depends on the details of the model, so as the CF. In what follows, we assume it is a sum of M decaying exponentials

$$\alpha(\tau) = \sum_{j=1}^{M} G_j \, e^{-i\omega_j \tau - \kappa_j |\tau|}, \tag{2}$$

with κ_j, ω_j, $G_j \in \mathbb{R}$. This decomposition can be performed in a wide range of applications, either exactly or with great precision [19, 29–31]. This amounts to decomposing the non-Markovian structured environment E into a set of M modes of frequencies $\{\omega_j\}$ which are damped with rates $\{\kappa_j\}$ due to their coupling to independent Markovian baths, as illustrated in Fig. 1. This so-called pseudo-mode picture [32–39] can be applied to a wide range of systems, from atoms in a lossy cavity, to superconducting qubits coupled to leaky resonators [40, 41], electrons coupled to damped phonons [42, 43], or emitters in plasmonic cavities [44]. The form (2) of the CF with the assumption that the global system is initially in the product state $\rho(0) = \rho_S(0) \otimes \rho_B(0)$ allows us to describe the complete dynamics of our model via a numerically exact method called the hierarchical equations of motion (HEOM) which takes the form [15–19]

$$\begin{aligned}\frac{d\rho^{(\vec{n},\vec{m})}}{dt} &= -i[H_S, \rho^{(\vec{n},\vec{m})}] - (\vec{w}^* \cdot \vec{n} + \vec{w} \cdot \vec{m})\rho^{(\vec{n},\vec{m})} \\ &+ \sum_{j=1}^{M} \Big\{ G_j \left(n_j L_j \rho^{(\vec{n}-\vec{e_j},\vec{m})} + m_j \rho^{(\vec{n},\vec{m}-\vec{e_j})} L_j^\dagger \right) \\ &+ [\rho^{(\vec{n}+\vec{e_j},\vec{m})}, L_j^\dagger] + [L_j, \rho^{(\vec{n},\vec{m}+\vec{e_j})}] \Big\}, \end{aligned} \tag{3}$$

where $\vec{n} = (n_j)$ and $\vec{m} = (m_j)$ are multi-indices in $\mathbb{N}^M$, $\vec{w} = (\kappa_j + i\,\omega_j) \in \mathbb{C}^M$, $\vec{e_j} = (\delta_{jj'})$ unit vectors, and $\vec{a} \cdot \vec{b} = \sum_j a_j^* b_j$ the standard scalar product in $\mathbb{C}^M$. In Eq. (3), $\rho^{(\vec{0},\vec{0})} \equiv \rho_S$ corresponds to the physical density operator of the system S with which all the system correlations are computed, while $\rho^{(\vec{n},\vec{m})}$ for $(\vec{n},\vec{m}) \neq (\vec{0},\vec{0})$, which are also operators acting on the system Hilbert space $\mathcal{H}_S$, correspond to auxiliary states from which bath correlations can be obtained [10]. Although the hierarchy is formally infinite, it can be truncated in practice at large hierarchy depth indices $\vec{n}$ and $\vec{m}$. In general, the stronger the non-Markovianity, the larger the number of auxiliary states we need to retain to obtain convergence of the results. Here, we choose a triangular truncation condition such that $\rho^{(\vec{n},\vec{m})}(t) = 0 \;\forall\, \vec{n},\vec{m} : \sum_j (n_j + m_j) > k_{\max}$, where $k_{\max}$ is the truncation order, yielding a total of $K = (2M + k_{\max})!/((2M)!\,k_{\max}!)$ auxiliary states [10].

An effective non-Markovian Liouvillian matrix can be derived by exploiting the Choi-Jamiołkowski isomorphism between linear maps and states [45]. Vectorizing (3) with $|i\rangle\langle j| \cong |i\rangle \otimes |j\rangle$, we get

$$\begin{aligned}&\frac{d|\rho^{(\vec{n},\vec{m})}\rangle\!\rangle}{dt} \\ &= -i\left[H_S \otimes \mathbb{1} - \mathbb{1} \otimes H_S^T - (\vec{w} \cdot \vec{n} + \vec{w}^* \cdot \vec{m})\right] |\rho^{(\vec{n},\vec{m})}\rangle\!\rangle \\ &+ \sum_{j=1}^{M} G_j \left(n_j L_j \otimes \mathbb{1} |\rho^{(\vec{n}-\vec{e_j},\vec{m})}\rangle\!\rangle + m_j \mathbb{1} \otimes L_j^* |\rho^{(\vec{n},\vec{m}-\vec{e_j})}\rangle\!\rangle \right) \\ &+ \sum_{j=1}^{M} \Big[(\mathbb{1} \otimes L_j^* - L_j^\dagger \otimes \mathbb{1}) |\rho^{(\vec{n}+\vec{e_j},\vec{m})}\rangle\!\rangle \\ &\qquad - (\mathbb{1} \otimes L_j^* - L_j^\dagger \otimes \mathbb{1})^\dagger |\rho^{(\vec{n},\vec{m}+\vec{e_j})}\rangle\!\rangle \Big], \end{aligned} \tag{4}$$

where $|\rho^{(\vec{n},\vec{m})}\rangle\!\rangle$ denotes the vectorization of the matrices $\rho^{(\vec{n},\vec{m})}$ and $\mathbb{1}$ the identity matrix acting on $\mathcal{H}_S$. We also used the notation L_j^* (L_j^T) for the conjugate (transpose) matrix of L_j. By stacking in a vector $|\rho\rangle\!\rangle$ all the vectorized matrices $|\rho^{(\vec{n},\vec{m})}\rangle\!\rangle$, we can construct a matrix $\mathcal{L}_{\rm HEOM}(k_{\max})$, called *HEOM's Liouvillian*, such that the system of linear equations (4) takes the form (see Supplemental Material (SM) for an example of explicit constructions of $\mathcal{L}_{\rm HEOM}$)

$$\frac{d|\rho\rangle\!\rangle}{dt} = \mathcal{L}_{\rm HEOM}(k_{\max})\,|\rho\rangle\!\rangle. \tag{5}$$

$\mathcal{L}_{\rm HEOM}(k_{\max})$ is the generator of the non-Markovian dynamics of the system which generalises Lindblad's Markovian Liouvillian. Equation (5) becomes *exact* for a CF of the form (2) in the limit $k_{\max} \to +\infty$. Alternatively, to obtain the dynamics of the system, we could enlarge it by including explicit bosonic degrees of freedom for the pseudo-modes and considering standard Lindblad damping channels for them, as illustrated in Fig. 1(b). This would define a standard Markovian Liouvillian $\mathcal{L}_M$ for the global system S_M. However, as

explained in the SM, using $\mathcal{L}_{\rm HEOM}$ is computationally more favorable than $\mathcal{L}_M$, especially for large M.

Properties of the HEOM's Liouvillian. The superoperator $\mathcal{L}_{\rm HEOM}$ is linear and in general non-Hermitian. We assume it is diagonalizable and denote its eigenvectors and eigenvalues by $|\rho_i\rangle\!\rangle$ and λ_i. For a truncation order $k_{\max}$, its dimension is $D = (2M + k_{\max})!\dim(\mathcal{H}_{\rm S})^2/[(2M)!k_{\max}!]$. It admits the following properties (see proofs in the SM): (i) its spectrum is symmetric with respect to the real axis; (ii) it preserves the trace of the physical state $\rho^{(\vec{0},\vec{0})}$; (iii) the eigenvalue 0 is always in its spectrum, guaranteeing the existence of a stationary state; (iv) all the eigenvalues must have a negative real part in the limit $k_{\max} \to +\infty$; (v) $\mathrm{Tr}[\mathbb{1}_{(\vec{0},\vec{0})}\rho_i] = 0$ if ρ_i is a right eigenoperator of $\mathcal{L}_{\rm HEOM}$ associated to the eigenvalue λ_i with $\mathrm{Re}[\lambda_i] \neq 0$. As in [4, 5], we order the eigenvalues of $\mathcal{L}_{\rm HEOM}$ so that $|\mathrm{Re}[\lambda_0]| < |\mathrm{Re}[\lambda_1]| < \cdots < |\mathrm{Re}[\lambda_D]|$, where $\lambda_0 = 0$.

DPT and HEOM's Liouvillian spectrum. Consider an open system dynamics described by Eq. (5) which admits a valid thermodynamic limit $N \to \infty$ and a unique steady state ρ_{ss} for all finite N. We say that the system undergoes a phase transition of order M when a non-analytical change in a g-independent system observable O occurs when the parameter g tends to a critical value g_c in the limit $N \to \infty$, i.e., [4]

$$\lim_{g\to g_c} \left| \frac{\partial^M}{\partial g^M} \lim_{N\to+\infty} \langle O\rangle_{ss} \right| = +\infty, \tag{6}$$

where $\langle O\rangle_{ss} = \mathrm{Tr}[O\rho_{ss}^{(\vec{0},\vec{0})}]$. This definition of DPTs is the same as for Markovian systems. The only difference is that the steady state is obtained from the HEOM (5) instead of the a Lindblad master equation. As for the Markovian case, a non-analytical change as described by (6) must occur due to a level crossing in the spectrum of $\mathcal{L}_{\rm HEOM}$, and thus to the closing of the HEOM's Liouvillian gap $\lambda \equiv |\mathrm{Re}[\lambda_1]|$.

Symmetries and DPTs. We call *weak symmetry* of $\mathcal{L}_{\rm HEOM}$ any unitary operator $\mathcal{U}$ such that $[\mathcal{L}_{\rm HEOM}, \mathcal{U}] = 0$. If $\mathcal{U}$ is a symmetry, then the matrix representing $\mathcal{L}_{\rm HEOM}$ in the eigenvector basis of $\mathcal{U}$ is block-diagonal

$$\mathcal{L}_{\rm HEOM} = \begin{bmatrix} \mathcal{L}_{u_0} & \cdots & 0 \\ \vdots & \ddots & \vdots \\ 0 & \cdots & \mathcal{L}_{u_n} \end{bmatrix}, \tag{7}$$

where each block $\mathcal{L}_{u_k}$ is associated with each distinct eigenvalue u_k of $\mathcal{U}$, in number $n+1$. We define the *symmetry sector* L_u as the subspace spanned by the eigenvectors of $\mathcal{U}$ associated with the eigenvalue u. Without any symmetry, all the $\rho^{(\vec{n},\vec{m})}$ states are coupled together by (3). In the presence of a symmetry $\mathcal{U}$, the Liouvillian is partitioned into uncoupled blocks and *independent* hierarchies for sets of components of the physical state $\rho^{(\vec{0},\vec{0})}$ can be written. We can prove that if the steady-state $|\rho_{ss}\rangle\!\rangle$ of (5) is unique, then $|\rho_{ss}\rangle\!\rangle \in L_{u=1}$ [46]. Again, in close analogy with the Markovian case [4], a DPT associated with a spontaneous symmetry breaking (SSB) is characterized by the occurrence of several eigenvectors, belonging to *different symmetry sectors*, associated with the same eigenvalue $\lambda = 0$ for $g \geq g_c$ if g (g_c) is the order parameter (its critical value) associated with the DPT. To be specific, if we assume that $\mathcal{L}_{\rm HEOM}$ can be written as a direct sum of $n+1$ blocks as in (7) and if the eigenvalues are sorted in each symmetry block k as $|\mathrm{Re}[\lambda_0^{(k)}]| < |\mathrm{Re}[\lambda_1^{(k)}]| < \cdots < |\mathrm{Re}[\lambda_{l(k)}^{(k)}]|$ (with $\sum_k l(k) = D$), a SSB in the thermodynamic limit is signaled by $\lambda_0^{(1)}, \lambda_0^{(2)}, \ldots, \lambda_0^{(n)} \to \lambda_0^{(0)} = 0$ for $g \geq g_c$ when $N \to +\infty$ [47]. Physically, this means that the independent hierarchies associated with each block mix in the limit $N \to +\infty$ so that ρ_{ss} is no longer an eigenvector of $\mathcal{U}$. Instead, ρ_{ss} becomes a statistical mixture of eigenvectors associated with *different symmetry sectors* for $g \geq g_c$. The existence of such a symmetry greatly simplifies the numerical computation, thanks to the block structure (7). The remainder of this work is devoted to the analysis of DPTs in experimentally relevant models where only Markovian dissipation regimes have been studied or where standard Lindblad descriptions fail.

First-order DPT. We first consider a Lipkin-Meshkov-Glick (LMG) model of the form

$$H_{\rm LMG} = \frac{V}{N}\left(S_x^2 - S_y^2\right) = \frac{V}{2N}\left(S_+^2 + S_-^2\right), \tag{8}$$

where $S_\alpha = \sum_{k=1}^N \sigma_\alpha^{(k)}/2$ ($\alpha = x, y, z$) are the collective spin operators defined in terms of N single-spin Pauli operators $\sigma_\alpha^{(k)}$ and $S_\pm = S_x \pm iS_y$. When the spin system undergoes collective decay as described by Lindblad's master equation

$$\dot{\rho} = -i[H_{\rm LMG}, \rho] + \frac{\gamma}{2N}\mathcal{D}[S_-] \tag{9}$$

where $\mathcal{D}[o] = 2o\rho o^\dagger - \{o^\dagger o, \rho\}$, as would occur if coupled to an unstructured bath, the model is known to exhibit a first order DPT at the critical point $V_c^{\rm M} = \gamma/2$ [28], separating a steady state phase where $\langle S_z\rangle/(N/2) \to -1$ for $N \to \infty$ ($V < V_c^{\rm M}$) to a phase where $\langle S_z\rangle/(N/2) \to 0$ ($V > V_c^{\rm M}$), as can be seen in Fig.2(a). For $V > V_c^{\rm M}$, a mean-field analysis predicts an infinite number of pure steady states corresponding to stable orbits on the Bloch sphere around fixed points located at the equator, yielding persistent oscillations of $\langle S_z\rangle$ that nonetheless averaged to zero over time [Fig.2(g)] [28]. Here, we generalize the study of this DPT to the non-Markovian regime by considering that the damping of the collective spin originates from the coupling of the system to a *structured* bath with a correlation function $\alpha(\tau) = G\, e^{-\kappa|\tau| - i\omega\tau}$, via an interaction Hamiltonian $H_{\rm int} = \sqrt{G}\,(S_- a^\dagger + S_+ a)$ with $G = \gamma\kappa/(2N)$ and a the annihilation operator of a

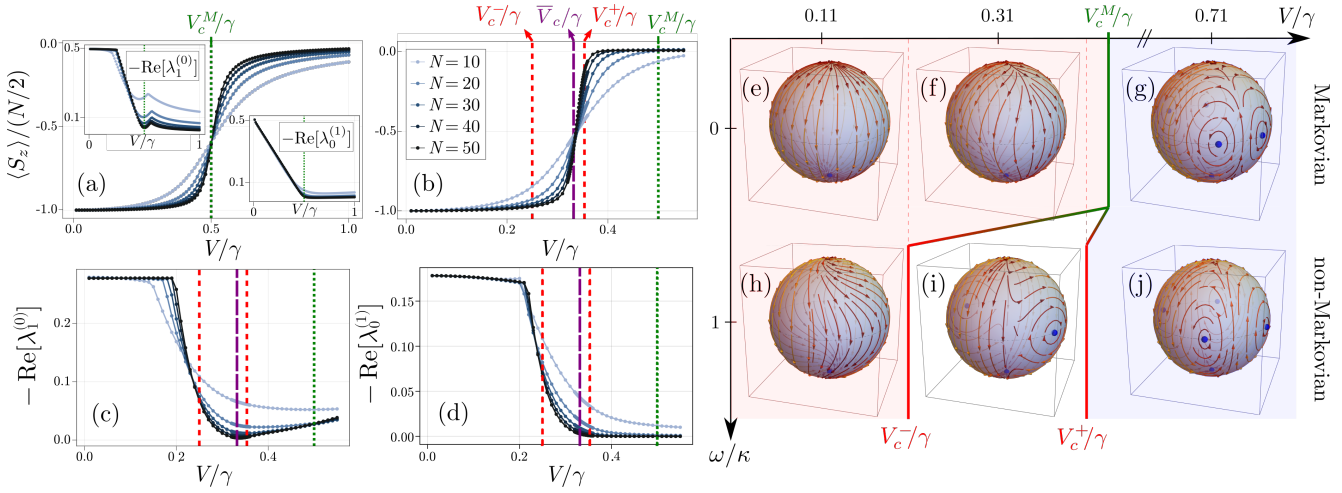

FIG. 2. Signatures of the first-order DPT for the generalized dissipative LMG model (8) obtained from $\mathcal{L}_{\mathrm{HEOM}}$, showing how environmental spectral structures affect the emergence of the DPT. (a,b): Steady state magnetization $\langle S_z\rangle/(N/2)$ as a function of V/γ for $\omega/\kappa = 50$ (a) and $\omega/\kappa = 1$ (b). The critical points are $V_c^- = 0.25\gamma$, $\overline{V}_c \approx 0.332\gamma$, $V_c^+ = 0.354\gamma$ for $\kappa = \gamma = \omega$. (c,d): Liouvillian gap $-\mathrm{Re}[\lambda_0^{(0)}]$ (c) and $-\mathrm{Re}[\lambda_0^{(1)}]$ (d) as a function of V/γ, indicating respectively the DPT and the SSB associated with the DPT. The insets of (a) show the same quantities for the Markovian case. Truncation orders are $k_{\max} = 2$ (a) and $k_{\max} = 6$ ($N = 10, 20, 30$), $k_{\max} = 7$ ($N = 40$), $k_{\max} = 9$ ($N = 50$) (b-d). (e-j) Stream plots showing the mean-field pure state trajectories of the collective spin on the Bloch sphere for $N \to \infty$ as a function of V/γ and of the degree of spectral density structures ω/κ. In the Markovian limit ($\omega/\kappa \to 0$), there is a phase transition at $V_c^M = 0.5\gamma$ between a phase with a unique pure steady state (blue dot at the south pole) [$V < V_c^M$, (e,f)] and a phase with an infinite set of (initial-state-dependent) pure steady states orbiting around four center fixed points (blue dots at the equator) [$V > V_c^M$, (g)]. As ω/κ increases, the stream lines twist around the z-axis (h) and a region of parameters ($V_c^- < V < V_c^+$) emerges where both the stable steady state at the south pole or a persistent oscillation can be observed depending on the initial condition (i). For $V > V_c^+$, only persistent oscillations remain (j).

damped pseudo-mode of Hamiltonian $H_E = \omega a^\dagger a$. This model allows us to study non-Markovian effects on the DPT and compare them to the Markovian case by tuning the "loss" rate κ of the pseudo-mode. Indeed, the collective spin and the pseudo-mode form an extended Markovian system governed by the master equation

$$\dot{\rho}_{\mathrm{tot}} = -i[H, \rho_{\mathrm{tot}}] + \kappa\, \mathcal{D}[a] \tag{10}$$

with $H = H_{\mathrm{LMG}} + H_E + H_{\mathrm{int}}$. Adiabatic elimination of the pseudo-mode's degrees of freedom recovers Eq. (9) in the limit $\kappa \to \infty$ (see SM). When κ is finite, memory effects arise and affect the DPT as described below. The model under consideration has a $\mathbb{Z}_2$ symmetry represented by the superoperator $\mathcal{U}_2 = U_2 \otimes U_2^\dagger$ with $U_2 = e^{i\pi(S_z + a^\dagger a)}$. $\mathcal{U}_2$ has two distinct eigenvalues $u_k = e^{ik\pi} = \pm 1$ with $k = 0, 1$ and so there are two sectors of symmetry associated with the parity of the total number of excitations, with $L_{u_0=1}$ containing ρ_{ss}.

The impact of memory effects on the DPT based on the study of the non-Markovian Liouvillian $\mathcal{L}_{\mathrm{HEOM}}$ for the spin system can be seen in Fig. 2. First, we see in panel (b) that the steady state spin magnetization $\langle S_z\rangle$ exhibits a transition at a critical point $\overline{V}_c$ smaller than in the Markovian case shown in Fig. 2(a). A mean-field analysis (10) provides an explanation of this observation (see SM for all details). In a nutshell, the fully polarized steady state yielding $\langle S_z\rangle/(N/2) \to -1$ becomes unstable for $V > V_c^+ = \gamma/(2\sqrt{1+\omega^2/\kappa^2})$, while the fixed points at the Bloch sphere equator become unstable only for $V < V_c^- = \gamma/(2(1+\omega^2/\kappa^2))$. For $V_c^- < V < V_c^+$, a new phase emerges where both the fully polarized state at the south pole and orbits around the fixed points can be valid steady states, as can be seen in panel (i). For $V \gtrsim V_c^-$, only orbits closed to the fixed points are stable. As V increases, more orbits become stable, meaning that the mean-field critical point depends on the initial conditions on the Bloch sphere. As the HEOM's Liouvillian describes the statistical behavior of the system, it predicts the transition at the averaged mean-field critical points, which for $\omega/\kappa = 1$ is $\overline{V}_c/\gamma \approx 0.332$ (see SM).

From a physical point of view, the shift in the critical point can be understood as follows: the smaller κ, the greater the probability that excitations escaping from the system will be reabsorbed by the system at later times. The degree of openness of the system therefore decreases as κ decreases, which leads to a stabilisation of the phase dominated by the Hamiltonian (8) for small values of V. In the limit $\kappa \to 0$ (*i.e.* for a closed system), the phase transition disappears because the Hamiltonian dynamics no longer competes with dissipative dynamics. In the opposite limit $\kappa \to \infty$, we recover the Markovian case as $V_c^\pm, \overline{V}_c \to V_c^{\mathrm{M}}$. The HEOM's Liouvillian spectrum cor-

rectly captures all DPT signatures. Indeed, it captures the emergence of both the level-touching at the critical point in the symmetry sector $k = 0$, i.e., $-\mathrm{Re}[\lambda_0^{(0)}] \to 0$ at $V = \overline{V}_c$ as $N \to \infty$ (a necessary and sufficient condition for a first-order DPT) and the SSB associated to the DPT, i.e., $-\mathrm{Re}[\lambda_0^{(1)}] \to 0$ for $V \geq \overline{V}_c$ as $N \to \infty$. These features can be seen in panels (c) and (d).

Note that this DPT can be studied via an approximate reduced description of the collective spin dynamics, by performing an adiabatic elimination of the pseudo-mode (see [13] for a similar approach for the Dicke model). However, this approach gives incorrect quantitative results for finite N, which prevents finite-size effects from being estimated correctly. Also, it cannot always account for all the features of a DPT, as discussed in the next section, which motivates the use of our framework.

Second order DPT. We now examine the case of a second order DPT with SSB in a model for which the reduced Redfield descriptions (to order 2 and 4) of the system fail to capture the relaxation dynamics correctly: a two-mode Dicke model described by [14, 48]

$$H = \omega_0 S_z + \omega_A a^\dagger a + \omega_B b^\dagger b + \frac{g}{\sqrt{N}}(aS_+ + bS_- + \text{h.c.}), \quad (11)$$

where $S_z, S_\pm$ are collective spin operators and a, b ($a^\dagger$, $b^\dagger$) bosonic annihilation (creation) operators, to which we add damping of the modes a and b at the same rate κ yielding the Lindblad master equation (11)

$$\dot{\rho}_{\mathrm{tot}} = -i[H, \rho_{\mathrm{tot}}] + \kappa(\mathcal{D}[a] + \mathcal{D}[b]). \quad (12)$$

This model is known to undergo a second-order DPT between a normal phase with $\langle a \rangle = \langle b \rangle = 0, |\langle S_z \rangle| = N/2$ and a superradiant phase with $\langle a \rangle, \langle b \rangle \neq 0, |\langle S_z \rangle| < N/2$ as $N \to \infty$ [48]. For $\omega_A = \omega_B = \omega$, the critical value g_c of the coupling g that drives the transition can be calculated from a mean-field approach and satisfies $2g_c^2 N = \omega_0(\omega^2 + \kappa^2)/\omega$. The model (12) exhibits a continuous $\mathbb{U}(1)$ symmetry described by the superoperator $\mathcal{U}_1 = U_1 \otimes U_1^\dagger$ with $U_1 = e^{i\alpha(S_z + a^\dagger a - b^\dagger b)}$ ($\alpha \in \mathbb{R}$), spontaneously broken in the superradiant phase as $N \to \infty$.

Reduced descriptions of the collective spin dynamics have been studied and compared in [14] with the mean-field results summarized above. It has been shown that, unlike the previous dissipative LMG model (and the Dicke model [13]), a standard Redfield approach completely misses the DPT, while a fourth-order Redfield master equation (i.e., a fourth-order perturbative treatment in the interaction Hamiltonian) appears to capture the correct steady state and critical point but fails to predict the closing of the gap, a necessary condition for DPT. Our numerically exact and systematic method, on the other hand, captures all features of the DPT and the SSB, as shown in Fig. 3, which displays the magnetization $\langle S_z \rangle/(N/2)$ (a), the closing of the gap $|\mathrm{Re}[\lambda_0^{(k>0)}]|$ (c,d) and the imaginary part of $\lambda_0^{(k>0)}$ (b).

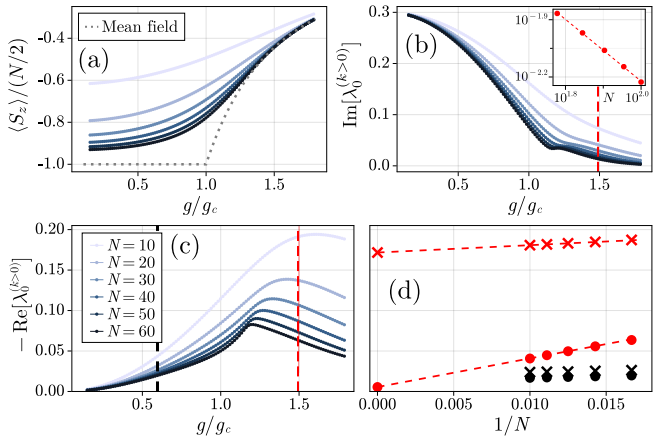

FIG. 3. Signatures of the second order DPT for the two-mode Dicke model (11) obtained from $\mathcal{L}_{\mathrm{HEOM}}$ for $\kappa = \omega = 5\omega_0$. (a): Steady state magnetization $\langle S_z \rangle /(N/2)$ as a function of g/g_c for $N = 10, 20, 30, 40, 50$ ($k_{\max} = 7$) and 60 ($k_{\max} = 8$). As N increases, the curves get closer to the mean-field result (dotted line). (b) Imaginary part $\lambda_0^{(k>0)}$ of the eigenvalue with the largest real part in the symmetry sector k that does not contain the steady state as a function of g/g_c, confirming the SSB. The inset shows the scaling of $\lambda_0^{(k>0)}$ as a function of N at $g/g_c = 1.49$. (c) $-\mathrm{Re}[\lambda_0^{(k>0)}]$ as a function of g/g_c showing a decreasing gap in the superradiant phase as N increases. The vertical dashed lines show the values $g/g_c = 1.49$ (red) and $g/g_c = 0.6$ (black) used in panel (d) to compare the scaling of $-\mathrm{Re}[\lambda_0^{(k>0)}]$ (circles) and of the Liouvillian gap of the 4^{th} Redfield master equation of [14] (crosses) as a function of $1/N$ [with $N = 60, 70, 80, 90$ ($k_{\max} = 8$) and 100 ($k_{\max} = 9$)]. In the normal phase (black), both methods are in good agreement, while in the superradiant phase (red), only $\mathcal{L}_{\mathrm{HEOM}}$ gives the expected closing. The points at $1/N = 0$ were extrapolated from a linear fit of the two last points of our data.

Conclusion. We developed a comprehensive framework for studying DPTs in arbitrary non-Markovian systems, relevant for realistic experimental conditions. Our method is numerically exact, systematic, easily implementable (as it is built on the well-established HEOM technique available in open access libraries [19, 20]), and provides a considerable computational advantage over a standard embedding technique. We first illustrated our method to characterize the impact of memory effects on a first-order DPT with a discrete SSB arising in a dissipative LMG model, and demonstrated that deviations from a flat environmental spectral density lead to a shift of the transition point, which could be observed e.g. in cavity QED or trapped ions. Secondly, we have shown that our method correctly captures all the defining features of a second-order DPT arising in a challenging $U(1)$-symmetric Dicke model for which other previously studied reduced descriptions had so far failed [14].

Our work makes it possible to explore out-of-equilibrium matter phases beyond the idealized Markovian limit, featuring non-markovianity as a resource for

controlling them. This is so far an unexplored territory as most works dealing with dissipative many-body dynamics is generally constrained to standard Lindblad dissipation, which potentially hinders the evidences of DPTs [13, 14]. Our method could be further improved via hybridization with advanced numerical techniques, such as corner-space renormalization [49] or matrix product operators (as in [43, 50–52]), to tackle DPTs in strongly interacting systems. Other perspectives include investigations in the non-Markovian regime of connections between DPTs and symmetry breaking [53, 54], geometric phase curvature [55, 56], or dynamical phase transitions [57, 58], measurement-induced phase transitions [59, 60], or dissipation engineering of long-range order [61].

Computational resources were provided by the Consortium des Equipements de Calcul Intensif (CECI), funded by the Fonds de la Recherche Scientifique de Belgique (F.R.S.-FNRS) under Grant No. 2.5020.11.

[1] J. Toner and Y. Tu, Phys. Rev. E **58**, 4828 (1998).
[2] J. Jin, A. Biella, O. Viyuela, L. Mazza, J. Keeling, R. Fazio, and D. Rossini, Phys. Rev. X **6**, 031011 (2016).
[3] T. E. Lee, S. Gopalakrishnan, and M. D. Lukin, Phys. Rev. Lett. **110**, 257204 (2013).
[4] F. Minganti, A. Biella, N. Bartolo, and C. Ciuti, Phys. Rev. A **98**, 042118 (2018).
[5] E. M. Kessler, G. Giedke, A. Imamoglu, S. F. Yelin, M. D. Lukin, and J. I. Cirac, Phys. Rev. A **86**, 012116 (2012).
[6] M.-J. Hwang, P. Rabl, and M. B. Plenio, Phys. Rev. A **97**, 013825 (2018).
[7] I. de Vega and D. Alonso, Rev. Mod. Phys. **89**, 015001 (2017).
[8] S. F. Huelga, A. Rivas, and M. B. Plenio, Phys. Rev. Lett. **108**, 160402 (2012).
[9] C. Maier, T. Brydges, P. Jurcevic, N. Trautmann, C. Hempel, B. P. Lanyon, P. Hauke, R. Blatt, and C. F. Roos, Phys. Rev. Lett. **122**, 050501 (2019).
[10] V. Link, K. Müller, R. G. Lena, K. Luoma, F. Damanet, W. T. Strunz, and A. J. Daley, PRX Quantum **3**, 020348 (2022).
[11] P. Chen, N. Yang, A. Couvertier, Q. Ding, R. Chatterjee, and T. Yu, Chaos and entanglement in non-markovian optomechanical systems (2023).
[12] F. Otterpohl, P. Nalbach, and M. Thorwart, Phys. Rev. Lett. **129**, 120406 (2022).
[13] F. Damanet, A. J. Daley, and J. Keeling, Phys. Rev. A **99**, 033845 (2019).
[14] R. Palacino and J. Keeling, Phys. Rev. Research **3**, L032016 (2021).
[15] Y. Tanimura and R. Kubo, Journal of the Physical Society of Japan **58**, 1199 (1989).
[16] A. Ishizaki and Y. Tanimura, Journal of the Physical Society of Japan **74**, 3131 (2005), https://doi.org/10.1143/JPSJ.74.3131.
[17] A. Ishizaki and G. R. Fleming, Proceedings of the National Academy of Sciences **106**, 17255 (2009), https://www.pnas.org/doi/pdf/10.1073/pnas.0908989106.
[18] Y. Tanimura, The Journal of Chemical Physics **153**, 020901 (2020), https://doi.org/10.1063/5.0011599.
[19] N. Lambert, T. Raheja, S. Cross, P. Menczel, S. Ahmed, A. Pitchford, D. Burgarth, and F. Nori, Qutip-bofin: A bosonic and fermionic numerical hierarchical-equations-of-motion library with applications in light-harvesting, quantum control, and single-molecule electronics (2020).
[20] Y.-T. Huang, P.-C. K. N. Lambert, M. Cirio, S. Cross, S.-L. Yang, F. Nori, and Y.-N. Chen, Heom.jl: An efficient julia framework for hierarchical equations of motion in open quantum systems (2023), arXiv:2306.07522 [quant-ph].
[21] D. Nagy and P. Domokos, Phys. Rev. Lett. **115**, 043601 (2015).
[22] D. Nagy and P. Domokos, Phys. Rev. A **94**, 10.1103/physreva.94.063862 (2016).
[23] P. Haikka, J. Goold, S. McEndoo, F. Plastina, and S. Maniscalco, Phys. Rev. A **85**, 060101 (2012).
[24] A. Strathearn, P. Kirton, D. Kilda, J. Keeling, and B. Lovett, Nature Communications **9** (2018).
[25] F. B. Anders, R. Bulla, and M. Vojta, Phys. Rev. Lett. **98**, 210402 (2007).
[26] A. W. Chin, J. Prior, S. F. Huelga, and M. B. Plenio, Phys. Rev. Lett. **107**, 160601 (2011).
[27] S. Florens, D. Venturelli, and R. Narayanan, Quantum phase transition in the spin boson model, in *Quantum Quenching, Annealing and Computation*, edited by A. K. Chandra, A. Das, and B. K. Chakrabarti (Springer Berlin Heidelberg, Berlin, Heidelberg, 2010) pp. 145–162.
[28] T. E. Lee, C.-K. Chan, and S. F. Yelin, Phys. Rev. A **90**, 052109 (2014).
[29] C. Meier and D. J. Tannor, The Journal of Chemical Physics **111**, 3365 (1999), https://doi.org/10.1063/1.479669.
[30] G. Ritschel and A. Eisfeld, The Journal of Chemical Physics **141**, 094101 (2014), https://doi.org/10.1063/1.4893931.
[31] R. Hartmann, M. Werther, F. Grossmann, and W. T. Strunz, The Journal of Chemical Physics **150**, 234105 (2019), https://doi.org/10.1063/1.5097158.
[32] A. Imamoglu, Phys. Rev. A **50**, 3650 (1994).
[33] B. J. Dalton, S. M. Barnett, and B. M. Garraway, Phys. Rev. A **64**, 053813 (2001).
[34] B. M. Garraway, Phys. Rev. A **55**, 2290 (1997).
[35] G. Pleasance, B. M. Garraway, and F. Petruccione, Phys. Rev. Research **2**, 043058 (2020).
[36] L. Mazzola, S. Maniscalco, J. Piilo, K.-A. Suominen, and B. M. Garraway, Phys. Rev. A **80**, 012104 (2009).
[37] H. Yang, H. Miao, and Y. Chen, Phys. Rev. A **85**, 040101 (2012).
[38] H.-P. Breuer, Phys. Rev. A **70**, 012106 (2004).
[39] A. Barchielli, C. Pellegrini, and F. Petruccione, EPL (Europhysics Letters) **91**, 24001 (2010).
[40] S. Schmidt and J. Koch, Ann. Phys. **525**, 395 (2013).
[41] A. Blais, A. L. Grimsmo, S. M. Girvin, and A. Wallraff, Rev. Mod. Phys. **93**, 025005 (2021).
[42] S. Flannigan, F. Damanet, and A. J. Daley, Phys. Rev. Lett. **128**, 063601 (2022).
[43] M. Moroder, M. Grundner, F. Damanet, U. Schollwöck, S. Mardazad, S. Flannigan, T. Köhler, and S. Paeckel, Phys. Rev. B **107**, 214310 (2023).
[44] K. Santhosh, O. Bitton, L. Chuntonov, and G. Haran, Nature Communications **7** (2015).
[45] M. Zwolak and G. Vidal, Phys. Rev. Lett. **93**, 207205 (2004).

[46] Indeed, by definition of the steady-state, we have $\mathcal{L}_{\rm HEOM}|\rho_{ss}\rangle\rangle = 0$, from which we get $\mathcal{U}\mathcal{L}_{\rm HEOM}|\rho_{ss}\rangle\rangle = \mathcal{L}_{\rm HEOM}\mathcal{U}|\rho_{ss}\rangle\rangle = 0$ by definition of the symmetry. Since $|\rho_{ss}\rangle\rangle$ is unique, we must have $\mathcal{U}|\rho_{ss}\rangle\rangle = |\rho_{ss}\rangle\rangle$, which shows that $|\rho_{ss}\rangle\rangle \in L_{u=1}$.

[47] F. Minganti, V. Savona, and A. Biella, Dissipative phase transitions in n-photon driven quantum nonlinear resonators (2023), arXiv:2303.03355 [quant-ph].

[48] R. I. Moodie, K. E. Ballantine, and J. Keeling, Phys. Rev. A **97**, 033802 (2018).

[49] S. Finazzi, A. Le Boité, F. Storme, A. Baksic, and C. Ciuti, Phys. Rev. Lett. **115**, 080604 (2015).

[50] E. Mascarenhas, H. Flayac, and V. Savona, Phys. Rev. A **92**, 022116 (2015).

[51] J. Cui, J. I. Cirac, and M. C. Bañuls, Phys. Rev. Lett. **114**, 220601 (2015).

[52] S. Flannigan, F. Damanet, and A. J. Daley, arXiv (2021).

[53] J. Huber, P. Kirton, and P. Rabl, Phys. Rev. A **102**, 012219 (2020).

[54] F. Minganti, I. I. Arkhipov, A. Miranowicz, and F. Nori, New Journal of Physics **23**, 122001 (2021).

[55] A. Carollo, D. Valenti, and B. Spagnolo, Physics Reports **838**, 1 (2020), geometry of quantum phase transitions.

[56] A. Carollo, B. Spagnolo, and D. Valenti, Scientific Reports **8** (2018).

[57] T. H. Kyaw, V. M. Bastidas, J. Tangpanitanon, G. Romero, and L.-C. Kwek, Phys. Rev. A **101**, 012111 (2020).

[58] D. Dolgitzer, D. Zeng, and Y. Chen, Opt. Express **29**, 23988 (2021).

[59] M. Buchhold, Y. Minoguchi, A. Altland, and S. Diehl, Phys. Rev. X **11**, 041004 (2021).

[60] T. Müller, S. Diehl, and M. Buchhold, Phys. Rev. Lett. **128**, 010605 (2022).

[61] J. Tindall, B. Buča, J. R. Coulthard, and D. Jaksch, Phys. Rev. Lett. **123**, 030603 (2019).

Supplemental Material: Spectral Theory of Non-Markovian Dissipative Phase Transitions

Baptiste Debecker, John Martin, François Damanet
Institut de Physique Nucléaire, Atomique et de Spectroscopie, CESAM, University of Liège, B-4000 Liège, Belgium

This Supplemental Material provides analytical and numerical details on the results presented in the main text of "Spectral Theory of Non-Markovian Dissipative Phase Transitions". In Sec. I, we first provide an example of explicit constructions of the HEOM's Liouvillian $\mathcal{L}_{\text{HEOM}}$. In Sec. II, we give a general argument on the computational advantage of using $\mathcal{L}_{\text{HEOM}}$ over the standard Markovian embedding technique illustrated in Fig. 1 of the main text. In Sec. III, we give the proofs of the properties of $\mathcal{L}_{\text{HEOM}}$ stated in the main text. In Sec. IV, we provide details on the first-order DPT in the Lipkin-Meshkov-Glick model. Finally, in Sec. V, we present convergence analyses of our method for the two models investigated in the main text, which we compare with the enlarged Markovian system technique.

CONTENTS

I. EXPLICIT MATRIX FORM OF THE HEOM'S LIOUVILLIAN

For the sake of clarity, we explicitly construct the different blocks of the matrix representation of the HEOM's Liouvillian for an environment made of only one damped pseudo-mode ($M = 1$). For this special case, the vectorized HEOM reads

$$\begin{aligned}\frac{d|\rho^{(\vec{n},\vec{m})}\rangle\!\rangle}{dt} = &\underbrace{\left[-i\left(H_S\otimes\mathbb{1}-\mathbb{1}\otimes H_S^T\right)-((n-m)i\omega_c+(n+m)\kappa)\mathbb{1}\otimes\mathbb{1}\right]}_{\equiv D_{nm}}|\rho^{(n,m)}\rangle\!\rangle\\ &+\underbrace{(Gn\ L\otimes\mathbb{1})}_{\equiv A_n}|\rho^{(n-1,m)}\rangle\!\rangle+\underbrace{(Gm\ \mathbb{1}\otimes L^*)}_{\equiv B_m}|\rho^{(n,m-1)}\rangle\!\rangle\\ &+\underbrace{(\mathbb{1}\otimes L^*-L^\dagger\otimes\mathbb{1})}_{\equiv C}|\rho^{(n+1,m)}\rangle\!\rangle+\underbrace{(L\otimes\mathbb{1}-\mathbb{1}\otimes L^T)}_{\equiv -C^\dagger}|\rho^{(n,m+1)}\rangle\!\rangle.\end{aligned}$$

Therefore, if $k_{\max}=1$ the stacked vector $|\rho\rangle\!\rangle$ is given by $|\rho\rangle\!\rangle=(|\rho^{(0,0)}\rangle\!\rangle,|\rho^{(0,1)}\rangle\!\rangle,|\rho^{(1,0)}\rangle\!\rangle)^T$ and

$$\mathcal{L}_{\mathrm{HEOM}}(k_{\max}=1)=\begin{pmatrix} D_{00} & -C^\dagger & C \\ B_1 & D_{01} & 0 \\ A_1 & 0 & D_{10}\end{pmatrix}, \tag{S1}$$

while for $k_{\max}=2$, we get $|\rho\rangle\!\rangle=(|\rho^{(0,0)}\rangle\!\rangle,|\rho^{(0,1)}\rangle\!\rangle,|\rho^{(0,2)}\rangle\!\rangle,|\rho^{(1,0)}\rangle\!\rangle,|\rho^{(1,1)}\rangle\!\rangle,|\rho^{(2,0)}\rangle\!\rangle)^T$ and

$$\mathcal{L}_{\mathrm{HEOM}}(k_{\max}=2)=\begin{pmatrix} D_{00} & -C^\dagger & 0 & C & 0 & 0 \\ B_1 & D_{01} & -C^\dagger & 0 & C & 0 \\ 0 & B_2 & D_{02} & 0 & 0 & 0 \\ A_1 & 0 & 0 & D_{10} & -C^\dagger & C \\ 0 & A_1 & 0 & B_1 & D_{11} & 0 \\ 0 & 0 & 0 & A_2 & 0 & D_{20}\end{pmatrix}. \tag{S2}$$

II. COMPUTATIONAL ADVANTAGE OF $\mathcal{L}_{\mathrm{HEOM}}$ - GENERAL ARGUMENT

In this section, we compare the dimension of the HEOM Liouvillian $\mathcal{L}_{\mathrm{HEOM}}$ to the one of the Liouvillian for the enlarged Markovian system that includes the pseudomodes, which we denote by $\mathcal{L}_{\mathrm{M}}$. This provides an overall idea of what kind of computational advantage of using $\mathcal{L}_{\mathrm{HEOM}}$ instead of $\mathcal{L}_{\mathrm{M}}$ can be expected. A more detailed comparison for the LMG model investigated in the main text can be found in Sec. V.

The dimension of the matrix representing $\mathcal{L}_{\mathrm{HEOM}}$ is

$$D=\dim\left(\mathcal{L}_{\mathrm{HEOM}}\right)=\frac{(2M+k_{\max})!}{(2M)!k_{\max}!}\dim(\mathcal{H}_{\mathrm{S}})^2 \tag{S3}$$

It depends on the size of the system Hilbert space $\mathcal{H}_S$, and of the truncation order $k_{\max}$ and the number of pseudo modes M which determines the number of auxiliary matrices of the hierarchy.

To compare with the dimension of the matrix representing the Liouvillian of the enlarged Markovian system $\mathcal{L}_{\mathrm{M}}$, we need to introduce a cutoff N_c for the pseudo-mode Fock spaces $\{|n_i\rangle\}$ ($n_i=0,1,\ldots,\infty$ and $i=1,2,\ldots,M$), which are in principle infinite. We choose here $N_c=k_{\max}$, motivated by the fact that the pseudo-mode correlation functions are related to the traces of the auxiliary matrices according to (for $M=1$) [S1]

$$\langle a^n(a^\dagger)^m\rangle=\frac{\mathrm{Tr}\left[\rho^{(n,m)}\right]}{(iG)^n(-iG)^m}, \tag{S4}$$

which means that if we truncate the hierarchy at $k_{\max}$, we need at least to truncate the pseudo-mode Fock space at $N_c=k_{\max}$ to be able to compute the same correlations. The dimension of $\mathcal{L}_{\mathrm{M}}$ should thus be

$$\dim\left(\mathcal{L}_{\mathrm{M}}\right)=\dim(\mathcal{H}_{\mathrm{S}})^2(k_{\max}+1)^M. \tag{S5}$$

The ratio $\dim\left(\mathcal{L}_{\mathrm{HEOM}}\right)/\dim\left(\mathcal{L}_{\mathrm{M}}\right)$ is plotted as a function of $k_{\max}$ and M in Fig. S1. We see that the advantage can be significant, especially for large numbers of pseudo-modes.

III. PROPERTIES OF THE HEOM'S LIOUVILLIAN

We provide here the proofs of the properties of the HEOM's Liouvillian. To show that the spectrum of $\mathcal{L}_{\mathrm{HEOM}}$ is symmetric with respect to the real axis, we note that $\left(\frac{d\rho^{(\vec{n},\vec{m})}}{dt}\right)^\dagger=\frac{d}{dt}\rho^{(\vec{m},\vec{n})}=\frac{d}{dt}(\rho^{(\vec{n},\vec{m})})^\dagger$, where we used the property $(\rho^{(\vec{n},\vec{m})})^\dagger=\rho^{(\vec{m},\vec{n})}$ [S1], implies $\mathcal{L}_{\mathrm{HEOM}}[\rho^\dagger]=(\mathcal{L}_{\mathrm{HEOM}}[\rho])^\dagger$. The trace preserving property of $\mathcal{L}_{\mathrm{HEOM}}$ is immediate from Eq. (3) of the main text. This implies that

$$\begin{aligned} 0&=\frac{d\mathrm{Tr}[\rho^{(\vec{0},\vec{0})}]}{dt}=\mathrm{Tr}\left[\frac{d}{dt}\rho^{(\vec{0},\vec{0})}\right]=\mathrm{Tr}\left[\mathbb{1}_{(\vec{0},\vec{0})}\ \mathcal{L}_{\mathrm{HEOM}}[\rho]\right] \\ &=\langle\!\langle\mathbb{1}_{(\vec{0},\vec{0})}|\mathcal{L}_{\mathrm{HEOM}}|\rho\rangle\!\rangle\quad\forall\ \rho, \end{aligned} \tag{S6}$$

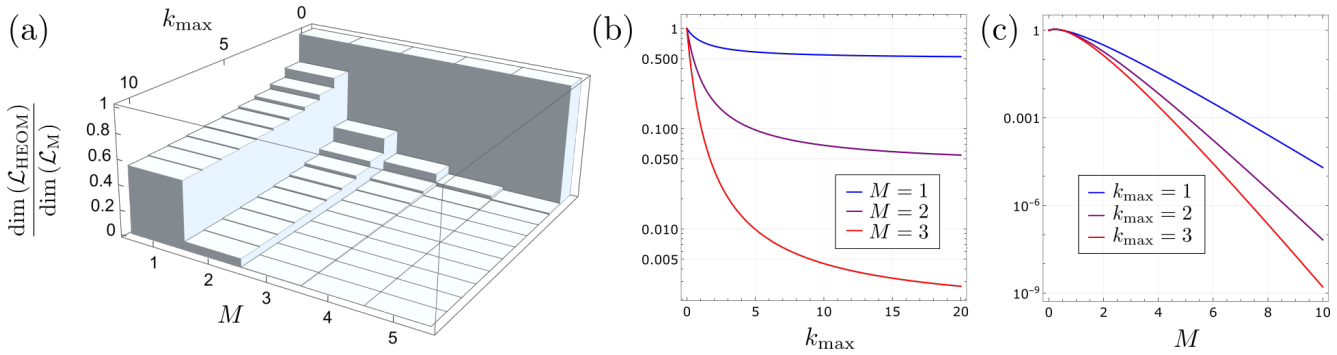

FIG. S1. Overall comparison between the dimensions of $\mathcal{L}_{\rm HEOM}$ and $\mathcal{L}_{\rm M}$: ratios $\dim(\mathcal{L}_{\rm HEOM})/\dim(\mathcal{L}_{\rm M})$ as a function $k_{\max}$ and M (a), as a function of $k_{\max}$ for $M=1,2$ and 3 (b), and as a function of M for $k_{\max}=1,2$ and 3 (c). Since $\dim(\mathcal{L}_{\rm HEOM})/\dim(\mathcal{L}_{\rm M})<1$, this means that we need less computational memory to store $\mathcal{L}_{\rm HEOM}$ than $\mathcal{L}_{\rm M}$.

where we used the Hilbert-Schmidt inner product $\langle\langle A|B\rangle\rangle \equiv \mathrm{Tr}[A^\dagger B]$ and the projector onto the physical state space $\mathbb{1}_{(\vec{0},\vec{0})}$. Equation (S6) leads to $\langle\langle \mathbb{1}_{(\vec{0},\vec{0})}|\mathcal{L}_{\rm HEOM}=0$, meaning that $\langle\langle \mathbb{1}_{(\vec{0},\vec{0})}|$ is a left eigenvector of $\mathcal{L}_{\rm HEOM}$ associated to the eigenvalue 0. Therefore, the eigenvalue 0 is always in the spectrum of $\mathcal{L}_{\rm HEOM}$, which guarantees the existence of a stationary state. The fact that all the eigenvalues must have a negative real part in the limit $k_{\max}\to+\infty$ comes from the fact that in this limit, the solution of Eq. (3) of the main text in the sector $(\vec{0},\vec{0})$ is *exactly* the reduced density operator of the system. Thus, any positive real part eigenvalues would lead to unphysical matrices in the sector $(\vec{0},\vec{0})$, therefore contradicting our last statement. Lastly, to prove that $\mathrm{Tr}[\mathbb{1}_{(\vec{0},\vec{0})}\rho_i]=0$ if ρ_i is a right eigenoperator of $\mathcal{L}_{\rm HEOM}$ associated to the eigenvalue λ_i with $\mathrm{Re}[\lambda_i]\neq 0$, we note that $\mathcal{L}_{\rm HEOM}$ preserves the trace in the sector $(\vec{0},\vec{0})$ and $\rho_i(t)=e^{\mathcal{L}_{\rm HEOM}t}\rho_i\to 0$ for $t\to+\infty$ if $\mathrm{Re}[\lambda_i]\neq 0$ and $k_{\max}\to+\infty$.

IV. FIRST-ORDER DISSIPATION PHASE TRANSITION

In this section, we present details on the generalized dissipative Lipkin-Meshkov-Glick model considered in the main text, which generalizes the study made in Ref. [S2] to the non-Markovian regime. The master equation for the collective spin and pseudo-mode density matrix reads [Eq. (10) in the main text]

$$\begin{aligned}\dot{\rho}_{\rm tot} &= -i\left[H,\rho_{\rm tot}\right]+\kappa\left(2a\rho_{\rm tot}a^\dagger-\{a^\dagger a,\rho_{\rm tot}\}\right)\\ \text{with}\qquad H &= H_{\rm LMG}+\omega a^\dagger a+\sqrt{\frac{\gamma\kappa}{2N}}\left(S_- a^\dagger+aS_+\right).\end{aligned}\tag{S7}$$

In the following, we first show how adiabatic elimination of the cavity mode recovers the original model [Eq.(9) in the main text] in the "bad cavity" limit before performing a mean-field analysis of our generalized model.

A. Adiabatic elimination of the cavity mode in the bad cavity limit

Let us perform a standard derivation of a Redfield master equation for the collective spin only, first dividing $H=H_0+H_1$ and then working in the interaction picture with respect to $H_0=H_{\rm LMG}+\omega a^\dagger a$. In this interaction picture, the interaction Hamiltonian H_1 takes the form:

$$H_1(t)=\sqrt{\frac{\gamma\kappa}{2N}}(a(t)S_+(t)+a^\dagger(t)S_-(t)),\tag{S8}$$

where $S_\pm(t)=e^{iH_{\rm LMG}t}S_\pm e^{-iH_{\rm LMG}t}$. The master equation for the collective spin density operator $\rho=\mathrm{Tr}_E(\rho_{\rm tot})$ reads in the Markov approximation [S3]:

$$\dot{\rho}=-\int_0^t dt'\mathrm{Tr}_E\left(\left[H_1(t),\left[H_1(t'),\rho\right]\right)\right).\tag{S9}$$

Considering the Born approximation $\rho_{\rm tot}(t) \approx \rho(t) \otimes \rho_E$ with ρ_E the vacuum state for the pseudo mode and expanding the double commutator makes appear the correlation function

$$\alpha(t-t') = \left(\frac{\gamma\kappa}{2N}\right) \mathrm{Tr}_E \left(a(t)a^\dagger(t')\rho_E\right) = \frac{\gamma\kappa}{2N} e^{-i\omega(t-t')-\kappa|t-t'|}. \tag{S10}$$

In the "bad cavity" limit $\kappa \to \infty$, we have $\alpha(t-t') \to (\gamma/N)\delta(t-t')$, which allows us to perform the integration straightforwardly and obtain the Redfield equation in the Schrödinger picture

$$\dot{\rho} = -i\left[H_{\rm LMG}, \rho\right] + \frac{\gamma}{2N}\left(2S_-\rho S_+ - \{S_+S_-, \rho\}\right) \tag{S11}$$

which is exactly Eq. (9) in the main text.

B. Mean-field analysis

1. Mean-field semiclassical equations of motions

We first start by writing the Heisenberg equations of motion for a, S_x, S_y and S_z from Eq. (S7)

$$\begin{aligned}
\dot{a} &= -(\kappa + i\omega)a - i\sqrt{\frac{\gamma\kappa}{2N}}S_- \\
\dot{S}_x &= -\frac{V}{N}\{S_y, S_z\} + i\sqrt{\frac{\gamma\kappa}{2N}}S_z(a - a^\dagger) \\
\dot{S}_y &= -\frac{V}{N}\{S_x, S_z\} - \sqrt{\frac{\gamma\kappa}{2N}}S_z(a + a^\dagger) \\
\dot{S}_z &= 2\frac{V}{N}\{S_x, S_y\} + i\sqrt{\frac{\gamma\kappa}{2N}}\left(a^\dagger S_- - aS_+\right)
\end{aligned} \tag{S12}$$

Using $\langle AB\rangle = \frac{1}{2}\left\langle\{A,B\} + [A,B]\right\rangle \approx \langle A\rangle\langle B\rangle + \frac{1}{2}\langle[A,B]\rangle$, we get the mean-field semiclassical equations of motion

$$\langle\dot{a}\rangle = -(\kappa + i\omega)\langle a\rangle - i\sqrt{\frac{\gamma\kappa}{2N}}\langle S_-\rangle \tag{S13}$$

$$\langle\dot{S}_x\rangle = -2\frac{V}{N}\langle S_y\rangle\langle S_z\rangle + i\sqrt{\frac{\gamma\kappa}{2N}}\langle S_z\rangle(\langle a\rangle - \langle a^\dagger\rangle) \tag{S14}$$

$$\langle\dot{S}_y\rangle = -2\frac{V}{N}\langle S_x\rangle\langle S_z\rangle - \sqrt{\frac{\gamma\kappa}{2N}}\langle S_z\rangle(\langle a\rangle) + \langle a^\dagger\rangle) \tag{S15}$$

$$\langle\dot{S}_z\rangle = 4\frac{V}{N}\langle S_x\rangle\langle S_y\rangle + i\sqrt{\frac{\gamma\kappa}{2N}}(\langle a^\dagger\rangle\langle S_-\rangle - \langle a\rangle\langle S_+\rangle), \tag{S16}$$

which are exact in the thermodynamic limit $N \to \infty$. In the following, we are interested in finding the fixed points of these equations and studying their stability as a function of the parameters of the model, in order to deduce the different possible steady states and build a phase diagram as in [S2].

2. Fixed points of the mean-field equations

The fixed points $\{(\langle a^*\rangle, \langle S_x^*\rangle, \langle S_y^*\rangle, \langle S_z^*\rangle)\}$ of Eqs. (S13)-(S16) can be obtained by setting the left-hand-side of all the equations to zero. In particular, from the first equation, setting $\langle\dot{a}\rangle = 0$ gives

$$\langle a^*\rangle = -i\frac{\sqrt{\frac{\gamma\kappa}{2N}}\langle S_-^*\rangle}{\kappa + i\omega}, \tag{S17}$$

i.e., slaving the pseudo-mode degree of freedom to the collective spin one, and makes it possible to obtain a closed set of equations for the collective spin variables $\langle S_x^*\rangle, \langle S_y^*\rangle$ and $\langle S_z^*\rangle$, i.e.,

$$0 = -2\frac{V}{N}\langle S_y^*\rangle\langle S_z^*\rangle + \frac{\gamma}{N}\langle S_z^*\rangle\left(q_1\langle S_x^*\rangle - q_2\langle S_y^*\rangle\right), \tag{S18}$$

$$0 = -2\frac{V}{N}\langle S_x^*\rangle\langle S_z^*\rangle + \frac{\gamma}{N}\langle S_z^*\rangle\left(q_1\langle S_y^*\rangle + q_2\langle S_x^*\rangle\right), \tag{S19}$$

$$0 = 4\frac{V}{N}\langle S_x^*\rangle\langle S_y^*\rangle - \frac{\gamma}{N}q_1\left(\langle S_x^*\rangle^2 + \langle S_y^*\rangle^2\right), \tag{S20}$$

where we introduced the factors

$$\begin{aligned} q_1 &= \frac{\kappa^2}{\kappa^2+\omega^2}, \\ q_2 &= \frac{\kappa\omega}{\kappa^2+\omega^2}. \end{aligned} \tag{S21}$$

It is worth noting that as an adiabatic elimination of the pseudo-mode also corresponds to setting $\dot{a} = 0$, a weak-coupling spin-only Redfield theory derived from Eq. (S7) would predict the exact fixed points, i.e., the Redfield theory is exact in the thermodynamic limit. Note also that in the limit $\kappa/\omega \to \infty$, we have $q_1 \to 1$ and $q_2 \to 0$ and we recover the semiclassical equations of the Lindblad model [S2]. Equations (S18)-(S20) together with the normalization condition $\langle S_x^*\rangle^2 + \langle S_y^*\rangle^2 + \langle S_z^*\rangle^2 = (N/2)^2$ admit as for the Markovian case two classes of fixed points:

$$\left(S_x^*, S_y^*, S_z^*\right) = \frac{N}{2}\left(0, 0, \pm 1\right) \tag{S22}$$

and

$$\left(S_x^*, S_y^*, S_z^*\right) = \frac{N}{2}\left(\frac{\sqrt{1\pm\sqrt{1-\frac{q_1^2\gamma^2}{4V^2}}}}{\sqrt{2}}, \frac{q_1\gamma}{4V}\frac{\sqrt{2}}{\sqrt{1\pm\sqrt{1-\frac{q_1^2\gamma^2}{4V^2}}}}, 0\right) \tag{S23}$$

$$\left(S_x^*, S_y^*, S_z^*\right) = -\frac{N}{2}\left(\frac{\sqrt{1\pm\sqrt{1-\frac{q_1^2\gamma^2}{4V^2}}}}{\sqrt{2}}, \frac{q_1\gamma}{4V}\frac{\sqrt{2}}{\sqrt{1\pm\sqrt{1-\frac{q_1^2\gamma^2}{4V^2}}}}, 0\right), \tag{S24}$$

In the following, we analyse the stability of these fixed points to determine the steady states of the model.

3. Linear stability analysis

Let us first perform a linear stability analysis around the first class of fixed points: $\left(S_x^*, S_y^*, S_z^*\right) = (0, 0, \pm N/2)$. To do so, we replace $\left(S_x^*, S_y^*, S_z^*\right)$ by $(x, y, z \pm (N/2))$ where (x, y, z) denotes fluctuations around the fixed points. Linearizing Eqs. (S18)-(S20) yields

$$\begin{pmatrix}\dot{x}\\ \dot{y}\\ \dot{z}\end{pmatrix} = \pm\frac{\gamma}{2}\begin{pmatrix} q_1 & -\frac{2V}{\gamma} - q_2 & 0 \\ -\frac{2V}{\gamma} + q_2 & q_1 & 0 \\ 0 & 0 & 0\end{pmatrix}\begin{pmatrix}x\\ y\\ z\end{pmatrix}. \tag{S25}$$

The eigenvalues of the matrix are 0, $\pm\gamma(q_1 - \sqrt{4(V/\gamma)^2 - q_2^2})/2$ and $\pm\gamma(q_1 + \sqrt{4(V/\gamma)^2 - q_2^2})/2$. For the fixed point $\left(S_x^*, S_y^*, S_z^*\right) = \left(0, 0, \frac{N}{2}\right)$, i.e., plus sign case above, the eigenvalue $\gamma(q_1 + \sqrt{4(V/\gamma)^2 - q_2^2})/2$ is always positive, meaning that it is always unstable. For the fixed point $\left(S_x^*, S_y^*, S_z^*\right) = \left(0, 0, -\frac{N}{2}\right)$, i.e., minus sign case above, the eigenvalue $-\gamma(q_1 - \sqrt{4(V/\gamma)^2 - q_2^2})/2$ is positive (and so the fixed point unstable) for

$$V > \frac{\gamma}{2\sqrt{1+\omega^2/\kappa^2}} \equiv V_c^+. \tag{S26}$$

To decide on the stability of the fixed point for $V < V_c^+$, we need to rely on a higher-order stability analysis because one of the eigenvalues of the matrix of the linear set of equations is zero, as elaborated on in the next subsection.

Similarly, let us perform a linear stability analysis around the second class of fixed points of the form $\left(S_x^*, S_y^*, S_z^*\right) = \left(s_x^*, s_y^*, 0\right)$, where s_x^* and s_y^* are given by the right-hand side of Eqs. (S23) or (S24). Here, the EOM for the fluctuations reads

$$\begin{pmatrix} \dot{x} \\ \dot{y} \\ \dot{z} \end{pmatrix} = \begin{pmatrix} 0 & 0 & q_1\gamma s_x^* - (2V + q_2\gamma)s_y^* \\ 0 & 0 & q_1\gamma s_y^* - (2V - q_2\gamma)s_x^* \\ 4Vs_y^* - 2q_1\gamma s_x^* & 4Vs_x^* - 2q_1\gamma s_y^* & 0 \end{pmatrix} \begin{pmatrix} x \\ y \\ z \end{pmatrix} + \begin{pmatrix} 0 \\ 0 \\ -\frac{N\gamma}{4} \end{pmatrix}. \tag{S27}$$

The eigenvalues are 0, $-N\sqrt{(\pm q_2\sqrt{4V^2 - \gamma^2 q_1^2} + \gamma^2 q_1^2 - 4V^2)/2}$ and $N\sqrt{(\pm q_2\sqrt{4V^2 - \gamma^2 q_1^2} + \gamma^2 q_1^2 - 4V^2)/2}$ for the fixed points of the form $\left(s_x^*, s_y^*, 0\right)$, where the $\pm$ sign relate to the $\pm$ sign in Eqs. (S23) and (S24. The fixed points are unstable as soon as the real part of these eigenvalues become positive. This happens for

$$V < \frac{\gamma}{2\left(1 + \omega^2/\kappa^2\right)} \equiv V_c^- \tag{S28}$$

for the two fixed points with the '-' sign in Eqs. (S23) and (S24) and for

$$V < V_c^+ \tag{S29}$$

for the two fixed points with the '+' sign.

While the linear stability analysis cannot provide a full understanding of the stability of the system, we already see strong deviations from the Markovian limit. Indeed, in this latter where $\omega/\kappa \to 0$, we have $V_c^- = V_c^+ = V_c^M = \gamma/2$ so that there is no region of parameters where the two kind of fixed points are not unstable, hampering the possibility for a coexistence of two distinct phases. More specifically, in [S2], it was shown that for $V < V_c^M$ the fixed point $(0, 0, -N/2)$ is the unique steady state while for $V > V_c^M$ the fixed points $\left(s_x^*, s_y^*, 0\right)$ are center fixed points and there exists an infinite set of oscillating (initial-state-dependent) steady states corresponding to orbits around these fixed points on the Bloch sphere. While these steady states are persistent spin oscillations, they average to zero along the z direction over time, so that the Markovian scenario well-describes a first-order transition between a phase with $\langle S_z\rangle \neq 0$ ($V < V_c^M$) and $\langle S_z\rangle = 0$ ($V > V_c^M$). In the non-Markovian case ($\omega/\kappa \neq 0$), however, we have $V_c^- < V_c^+$, so the possibility that the fixed points and thus two distinct phases coexist in this region of parameter (which increases as ω/κ increases) is not excluded. This is confirmed in the next section.

4. Higher-order stability analysis

As the equations of motion are cumbersome beyond linearization, we rely on a numerical analysis of the stability of the fixed points, as summarized below.

For $0 \leq V < V_c^-$, the fixed point $(0, 0, -N/2)$ is the unique steady state, as shown in the stream plots in Fig. S2 (a,b,e). Note that in this regime all the fixed points of the form $\left(s_x^*, s_y^*, 0\right)$ are not physical fixed points as they are complex vectors.

For $V_c^- < V < V_c^+$, we observe a bistability phenomenon as the steady state depends on the initial conditions: the fixed point $(0, 0, -N/2)$ is still a possible steady state, but an infinite number of steady states corresponding to stable orbits on the Bloch sphere around the two center fixed points (S23) and (S24) with the '-' sign become available, as shown in Fig. S2(f). For $V \gtrsim V_c^-$, only orbits close to the fixed points are stable. As V increases, more orbits become stable. This is in sharp contrast with the Markovian case where all the points on the sphere belong to stable orbits as soon as $V > V_c^M$ [panel (c,d)]. Here, in the regime $V_c^- < V < V_c^+$, each point on the Bloch sphere undergoes the phase transition at a different critical point. But as the HEOM's Liouvillian describes the statistical behaviour of the system, the critical point $\overline{V}_c$ observed in the main text corresponds to the mean of the critical points obtained from all possible pure state initial conditions. To show this, we numerically solved the set of Eqs S13-(S16) for a sample of 40000 random initial states on the Bloch sphere and computed for each of them the critical value V_c at which the average over time of $\langle S_z\rangle/(N/2)$ switches from -1 to 0. The histogram S3 shows the distributions of the critical points for $\omega/\kappa = 1$, that all lie between V_c^- and V_c^+. The distribution is almost flat everywhere, except at V_c^+ where there is a peak indicating that around half of the initial conditions lead to a critical point at V_c^+. The purple vertical line indicates the position of the mean of the critical points, which is $\overline{V}_c/\gamma \approx 0.332$ for $\omega/\kappa = 1$.

For $V > V_c^+$, the fixed point $(0, 0, -N/2)$ is no longer stable and all the four fixed points (S23) and (S24) become center fixed points, as can be seen in Fig. S2(g,h). Note that since $V_c^+ < V_c^M$, this means going beyond the limit of a flat spectral density has the effect to renormalize to lower values the critical point by a function of the bath SD. We

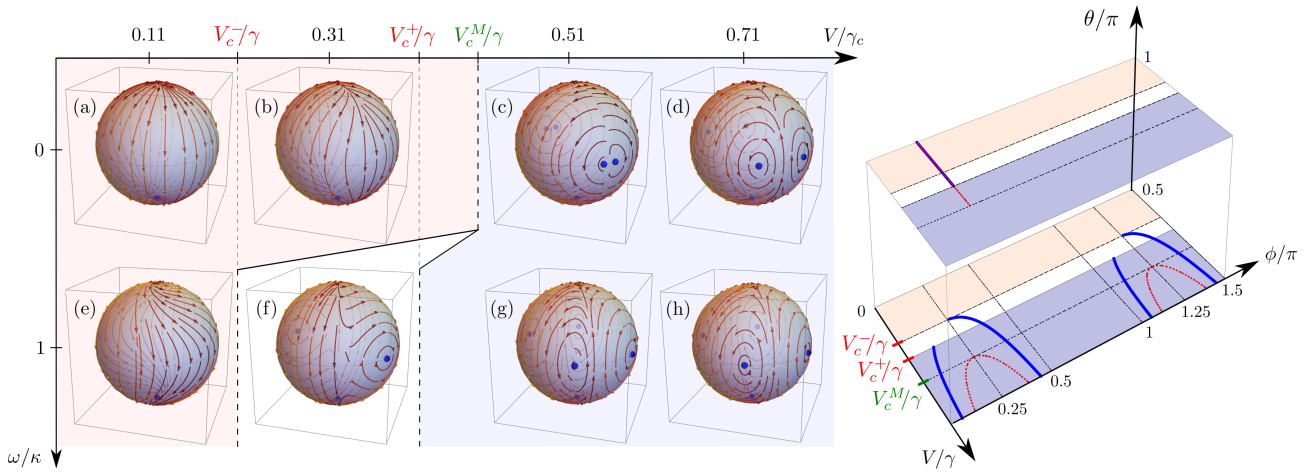

FIG. S2. Stream plots obtained from the mean-field equations (S13)-(S16) after adiabatic elimination of the cavity mode showing the trajectories of the collective spin on the Bloch sphere in the thermodynamic limit as a function of the ratio V/γ between coherent and dissipative rates (not in scale) and of the degree of spectral density structures ω/κ. In the Markovian limit ($\omega/\kappa \to 0$), there is a phase transition at $V = V_c^M = \gamma/2$ between a phase with a unique pure steady state $(0, 0, -N/2)$ (blue dot at the south pole) [$V < V_c^M$, (a,b)] and a phase with an infinite set of (initial-state-dependent) pure steady states orbiting around four center fixed points (blue dots at the equator) [$V > V_c^M$, (c,d)]. As ω/κ increases, the stream lines twist around the z-axis (e) and a region of parameters ($V_c^- < V < V_c^+$) emerges where both the steady state $(0, 0, -N/2)$ or a steady orbit can be observed depending on the initial condition (f). Overall, the phase space where the coherent dynamics dominates over the dissipative one is enlarged due to non-Markovian effects. Parameters are $V/\gamma = 0.11$ (a,e), $V/\gamma = 0.31$ (b,f), $V/\gamma = 0.51$ (c,g) and $V/\gamma = 0.71$ (d,h). For $\omega/\kappa = 1$, $V_c^-/\gamma = 0.25$ and $V_c^+/\gamma \approx 0.354$. (i) Positions of the relevant fixed points on the Bloch sphere as a function of spherical coordinates ϕ and θ and V/γ for the Markovian limit $\omega/\kappa = 0$ (dashed red) and for $\omega/\kappa = 1$ (blue).

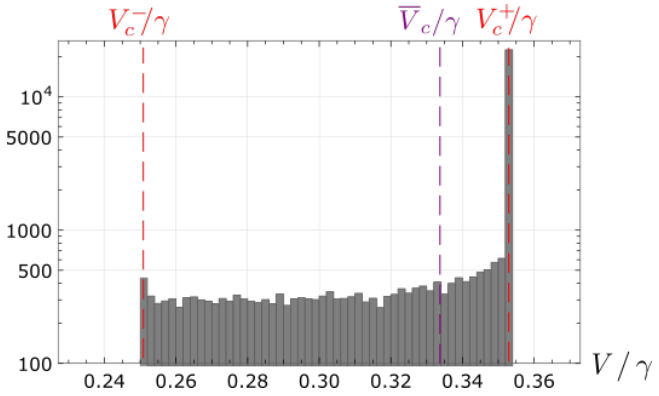

FIG. S3. Histogram showing the distribution of the critical points obtained from solving the time-dependent equations of motion (S13-S16) for a sample of 40000 random initial conditions uniformly distributed on the Bloch sphere for $\omega/\kappa = 1$. The vertical dashed lines indicate the positions of the critical points V_c^- and V_c^+ that constitute the lower and upper limit of the distribution, as well as the mean $\overline{V}_c$ of the critical points, which is the critical value predicted by $\mathcal{L}_{\text{HEOM}}$ in the main text.

interpret this phenomenon as a consequence of memory effects: for smaller κ/ω, the excitations escaping the system are more likely to be re-absorbed by the system at later times, protecting its coherence and hence stabilizing the phase dominated by the Hamiltonian term to lower ratio V/γ.

V. CONVERGENCE ANALYSIS AND NUMERICAL EFFICIENCY

The only parameter relevant to the convergence analysis of $\mathcal{L}_{\text{HEOM}}$ is the truncation order $k_{\max}$. We introduce the following measures of convergence

$$\begin{aligned} C_{k_{\max}}(O) &\equiv |\text{Tr}\left[\rho_{ss}(k_{\max})O - \rho_{ss}(k_{\max}+1)O\right]|\,, \\ S_{k_{\max}}(\lambda) &\equiv |\lambda(k_{\max}) - \lambda(k_{\max+1})|, \end{aligned} \tag{S30}$$

to assess the convergence of $\mathcal{L}_{\text{HEOM}}$ with respect to the steady state expectation value of a given operator O or with respect to one of its eigenvalue λ, such as the HEOM Liouvillian gap. Here, $\rho_{ss}(k_{\max})$ is the steady state of $\mathcal{L}_{\text{HEOM}}(k_{\max})$ and similarly $\lambda(k_{\max})$ is λ computed with $\mathcal{L}_{\text{HEOM}}(k_{\max})$. Note that the convergence measure $C_{k_{\max}}(O)$ is a natural choice often chosen to study the convergence of hierarchy of equations [S4]. The first part of this section is dedicated to the convergence analysis of $\mathcal{L}_{\text{HEOM}}(k_{\max})$ while the second part shed light on the numerical advantage of $\mathcal{L}_{\text{HEOM}}$ over enlarged Markovian systems.

A. Convergence analysis of $\mathcal{L}_{\text{HEOM}}(k_{\max})$

In Fig. S4, we show the two measures of convergence (S30) for the LMG model for $O = S_z$ [panels (a) and (b)] and $\lambda = \lambda_0^{(1)}$ [panels (c) and (d)]. As the hierarchy depth $k_{\max}$ increases, both measures of convergence $C_{k_{\max}}(S_z)$ and $S_{k_{\max}}(\lambda_0^{(1)})$ globally decrease, showing that the truncation order $k_{\max}$ can be used to control the numerical errors inherent to the $\mathcal{L}_{\text{HEOM}}(k_{\max})$ scheme. A comparison of the panels (a) and (c) with the panels (b) and (d) indicates that errors scale up as N increases. We also note that it is numerically more challenging to extract the spectral quantity $\lambda_0^{(1)}$ than the steady state expectation value $\langle S_z\rangle$, as indicated by the change in scale on the y-axis between panels (a) and (c) or (b) and (d).

These general observations still hold for the $\mathbb{U}(1)$-symmetric Dicke model of the main text, as illustrated in Fig S5, which is the analog of Fig S4 for the $\mathbb{U}(1)$-symmetric Dicke model. We note that both $C_{k_{\max}}(S_z)$ and $S_{k_{\max}}(\lambda_0^{(k>0)})$ increases as the coupling g increases, highlighting the numerical challenge of the so-called strong coupling regime. Moreover, this observation combined with the fact that the computation of $\lambda_0^{(k>0)}$ is numerically more demanding that of $\langle S_z\rangle$ could explain why a fourth order Redfield master equation seems to capture the right steady state but predicts a non-vanishing gap [S5]. We indeed foresee that the spectrum of $\mathcal{L}_{\text{HEOM}}$ converges faster for larger eigenvalues.

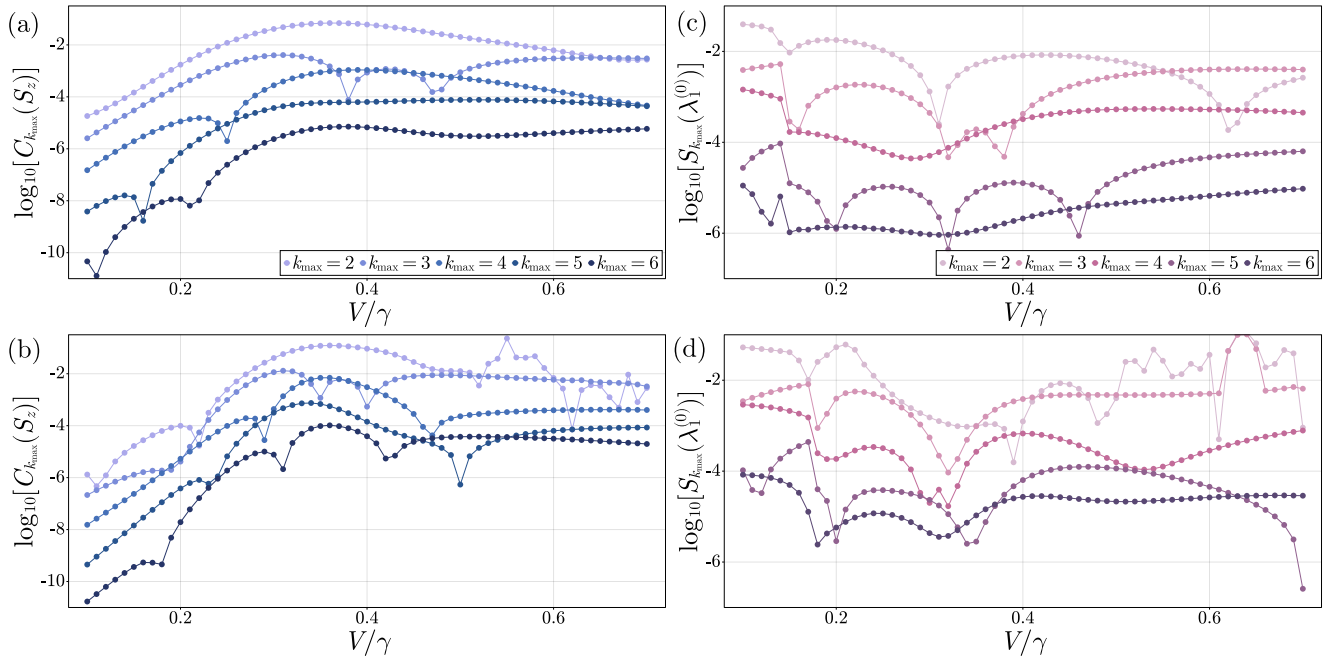

FIG. S4. Measures of convergence $C_{\max}(S_z)$ and $S_{k_{\max}}(\lambda_1^{(0)})$ as defined by Eq. (S30) for the LMG model discussed in the main text displayed in logarithmic scale as a function of V/γ. For all plots, the parameters are $\kappa = \omega = \gamma$ and $N = 10$ for panels (a) and (c) and $N = 20$ for panels (b) and (d).

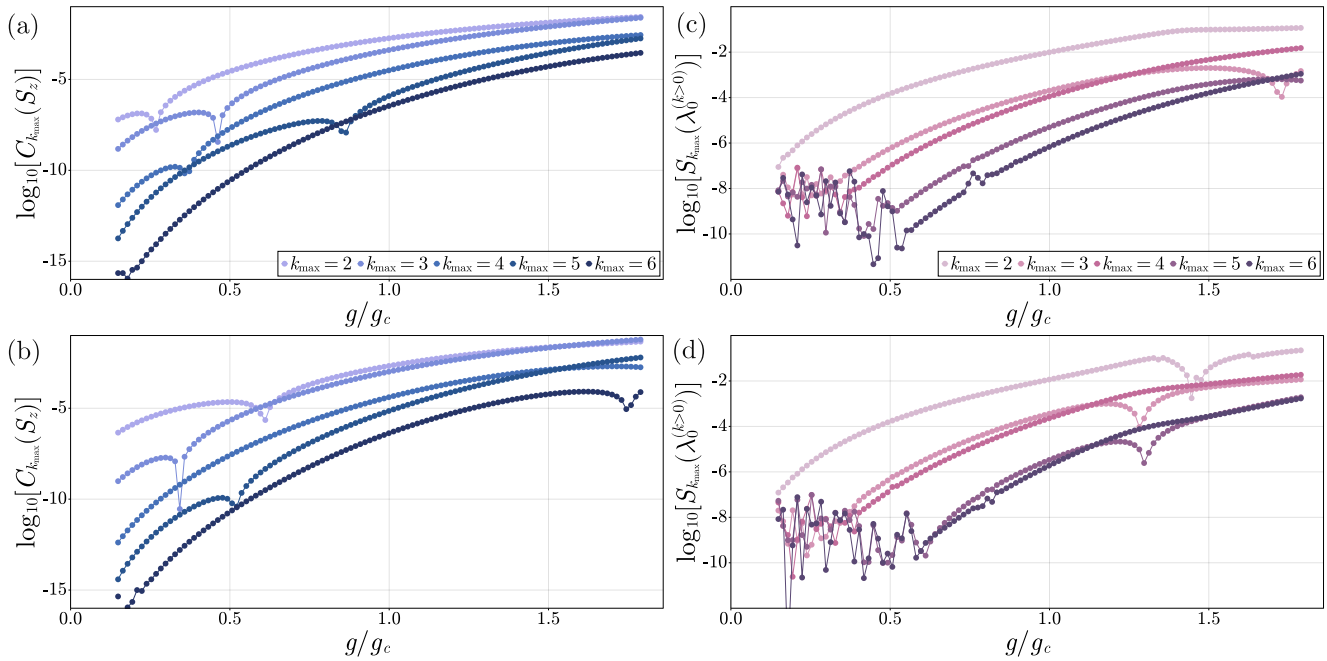

FIG. S5. Measures of convergence $C_{\max}(S_z)$ and $S_{k_{\max}}(\lambda_1^{(0)})$ as defined by Eq. (S30) for the $\mathbb{U}(1)$-symmetric Dicke model discussed in the main text displayed in logarithmic scale as a function of V/γ. For all panels, the parameters are $\kappa = \omega = 5\omega_0$ and $N = 10$ for panels (a) and (c) and $N = 20$ for panels (c) and (d).

B. Comparison with enlarged Markovian systems

Let us illustrate the numerical advantage of our method to characterize DPTs over the standard technique of analysing the spectrum of the Liouvillian for the enlarged Markovian system of the LMG model. For this model, this Markovian Liouvillian superoperator $\mathcal{L}_M$ is defined through

$$\dot{\rho}_{\rm tot} = -i\,[H, \rho_{\rm tot}] + \kappa\left(2a\rho_{\rm tot}a^\dagger - \{a^\dagger a, \rho_{\rm tot}\}\right) \equiv \mathcal{L}_M[\rho_{\rm tot}]. \tag{S31}$$

where $H = H_{\rm LMG} + \omega a^\dagger a + \sqrt{\frac{\gamma\kappa}{2N}}(S_- a^\dagger + S_+ a)$. As the dimension of $\mathcal{L}_M$ is infinite, one has to introduce a cutoff in order to determine the steady state of $\mathcal{L}_M$ numerically. We denote by N_c and $\mathcal{L}(N_c)$ the effective dimension of the truncated Fock space of the pseudo-mode and the associated truncated Markovian Liouvillian. In order to compare $\mathcal{L}_M$ and $\mathcal{L}_{\rm HEOM}$, we fix a threshold of tolerance for the measures of convergence, namely $\epsilon = 0.001$. We then choose $k_{\max}$ and N_c accordingly: we take the first value of $k_{\max}$ and N_c that satisfy

$$C_{k_{\max}}(S_z) < \epsilon \quad \text{and} \quad C_{N_c}(S_z) \equiv |\mathrm{tr}(\rho_{ss}(N_c)S_z - \rho_{ss}(N_c+1)S_z)| < \epsilon, \tag{S32}$$

where $\rho_{ss}(N_c)$ is the steady state associated with $\mathcal{L}_M(N_c)$. We then compute the effective dimension of $\mathcal{L}_M$ and $\mathcal{L}_{\rm HEOM}$ for the truncation parameters $k_{\max}$ and $\mathrm{N_c}$ previously determined. Figure S6(a) shows that the ratio $\dim(\mathcal{L}_{\rm HEOM})/\dim(\mathcal{L}_M)$ is below 0.4 for all V/γ and N considered. Moreover, this ratio decreases with N, which shows that the $\mathcal{L}_{\rm HEOM}$ scheme is more suited for the study of DPTs for which one must consider the thermodynamic limit $N \to +\infty$. Let us finally mention that the generators $\mathcal{L}_{\rm HEOM}$ and $\mathcal{L}_M$ give the same results at the chosen tolerance threshold as illustrated in Fig. S6(b).

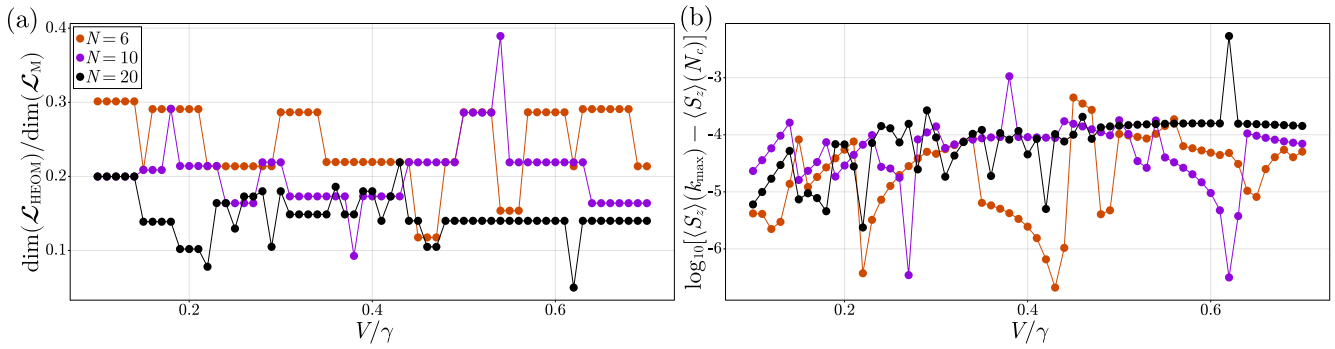

FIG. S6. Comparison of the convergence of $\mathcal{L}_{\mathrm{HEOM}}$ and $\mathcal{L}_{\mathrm{M}}$. (a): Ratio between the dimension of the HEOM generator $\mathcal{L}_{\mathrm{HEOM}}$ and the Markovian one $\mathcal{L}_{\mathrm{M}}$ as a function of V/γ for $\epsilon = 0.0001$, proving the numerical gain of using $\mathcal{L}_{\mathrm{HEOM}}$ instead of $\mathcal{L}_{\mathrm{M}}$ for the enlarged Markovian system. (b): Differences in logarithmic scale between the steady state expectation value $\langle S_z\rangle$ computed with $\mathcal{L}_{\mathrm{HEOM}}(k_{\max})$ (resp. $\mathcal{L}_{\mathrm{M}}(N_c)$) denoted by $\langle S_z\rangle(k_{\max})$ (resp. $\langle S_z\rangle(N_c)$) for $\epsilon = 0.0001$. The two methods are in good agreement at the given tolerance.

[S1] V. Link, K. Müller, R. G. Lena, K. Luoma, F. Damanet, W. T. Strunz, and A. J. Daley, PRX Quantum **3**, 020348 (2022).
[S2] T. E. Lee, C.-K. Chan, and S. F. Yelin, Phys. Rev. A **90**, 052109 (2014).
[S3] H.-P. Breuer and F. Petruccione, *The Theory of Open Quantum Systems* (Oxford University Press, Oxford, 2006).
[S4] D. Suess, A. Eisfeld, and W. T. Strunz, Phys. Rev. Lett. **113**, 150403 (2014).
[S5] R. Palacino and J. Keeling, Phys. Rev. Research **3**, L032016 (2021).